ELSEVIER

Nuclear Instruments and Methods in Physics Research A 454 (2000) 11–25

NUCLEAR INSTRUMENTS & METHODS IN PHYSICS RESEARCH Section A

www.elsevier.nl/locate/nima

Synchrotron light and imaging systems for medical radiology

Fulvia Arfelli*

Dipartimento di Fisica, Universita' di Trieste, Via A. Valerio 2, I-34127 Trieste, Italy

Abstract

In the past years several successful experimental studies have proven the suitability of synchrotron light in the field of medical radiology and in diagnostic medical imaging. To be mentioned and reviewed in the following are transvenous coronary angiography with synchrotron radiation, bronchography, single- or multi-energy tomography and synchrotron radiation-based mammography. Amongst those the most demanding application is X-ray mammography. Here, a dedicated system has to fulfil the demanding requirements on the source and the X-ray detector. Synchrotron radiation-based mammography, which enables improved image quality maintaining a low dose level, takes advantage of the tunable monochromatic energy and of the peculiar laminar geometry of the beam. In addition, further improvements can be achieved with the development of novel detectors for full-field digital mammography in order to overcome the intrinsic limitations of the conventional screen–film systems. Encouraging results in digital mammography have been obtained at the medical beamline of the synchrotron radiation facility ELETTRA, Trieste. Besides, the high degree of the spatial coherence of the synchrotron source allows new imaging modalities based on phase contrast effects that produce superior radiographs featuring highly enhanced contrast with a low delivered dose.

Keywords: Synchrotron radiation; Mammography; Digital imaging detectors; Phase imaging techniques

1. Introduction

Worldwide synchrotron radiation (SR) facilities provide an extraordinary kind of X-ray source, which offers a large variety of application in several fields such as material science, crystallography, micro-spectroscopy, X-ray diffraction and many others.

The main feature of these sources is the wide and continuous energy spectrum providing a very high photon flux over an energy range up to some 50 keV or even higher. Moreover, the beam comprises a high natural collimation at least in the vertical direction and a high degree of coherence in both, space and time. In the horizontal direction one can produce a large-area, fan-like photon beam shape.

All the aforementioned unique features in combination with the sophisticated optics make synchrotron sources well-suited instruments, e.g. for medical applications [1]. Thus during the past years several synchrotron radiation (SR) facilities have developed dedicated medical beamlines. They not only make use of the excellent source characteristics but also the fact that the high-intensity SR spectrum allows to select and tune monochromatic photon beams with a very narrow energy

* Corresponding author. Tel.: + 39-040-375-6233; fax: 39-040-375-6258.

E-mail address: arfelli@trieste.infn.it (F. Arfelli).

0168-9002/00/$ - see front matter
PII: S0168-9002(00)00803-2

bandwidth. As a consequence an enhancement of the image quality is observed while the dose is conserved or is even reduced at the same time. This is simply due to the fact that for each application the right energy window can be chosen. Besides the laminar geometry reduces scattered radiation and thus avoids image blurring. Moreover, the monochromaticity can be utilized to implement multiple energy techniques.

So far transvenous coronary angiography, computed tomography, bronchography and mammography have been implemented at several medical beamlines, just to mention some imaging applications.

A dedicated imaging system is required for each specific medical application and various approaches have been pursued with the development of different X-ray digital detectors with appropriate features like the geometry, the X-ray detection mode and the electronics. In general a high spatial detective quantum efficiency (DQE) close to 1 is essential for detectors used in medical radiology. Note, that $(1 - \mathrm{DQE})$ is the additional dose applied to the patient that does not contribute to an increase in image quality [2].

In particular in the last 10 years successful efforts have boosted the development of systems for clinical and synchrotron-based full-field digital mammography using different technologies.

Besides conventional radiography procedures new imaging modalities have been recently developed aiming at further improvement in the image quality based on the detection of phase shift information, an important effect especially for low absorbing biological materials.

2. Coronary angiography

Coronary angiography is a useful examination to reveal coronary artery disease that could lead to myocard infarct and subsequently even to death of the patient. Here the main interest is the visualization of occlusions (stenoses) in arteries down to a size of 1 mm in diameter. The conventional hospital procedure consists of an injection of an iodine-based contrast agent (with 370 mg/ml iodine) directly into the coronary arterial system via catheter while an X-ray transmission image/video is taken. As a screening procedure, however, this method is not useful since it bears a high risk (even death in up to 0.1% of the examinations depending on the age and the health condition [3]) due to the insertion of the catheter.

SR-based transvenous coronary angiography (certainly the most advanced SR-based medical program) is a less invasive method since the contrast agent is injected in the veins with a sensible reduction of risk. On its travel through the venous system and subsequently through the lungs the iodine bolus is rather diluted (around 10 mg/ml). Using conventional equipment this method turns out to be unsuitable for imaging fast moving objects like the heart and only a SR source can provide sufficient photon intensity in order to obtain a reasonable contrast between small arteries and the surrounding areas.

Basically the set-up (Fig. 1) consists of two monoenergetic photon beams bracketing the iodine K-edge and intersecting at the heart position. Two images are taken simultaneously by a dual line digital detector while the patient is translated in vertical direction through the cross-over point of the fan beams. In order to avoid artifact due to the movement of the heart the scan should be completed within 250 ms. Once the images are taken a digital logarithmic subtraction on a pixel base is performed that allows to extract the iodine signal (Fig. 2). The following algorithm (1) is based on the (simplified) assumption that the patient consists only of water and iodine [4]. In this fashion one

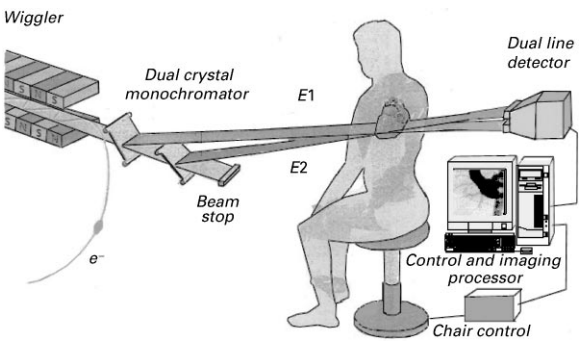

Fig. 1. The typical experimental set-up for transvenous coronary angiography with synchrotron radiation.

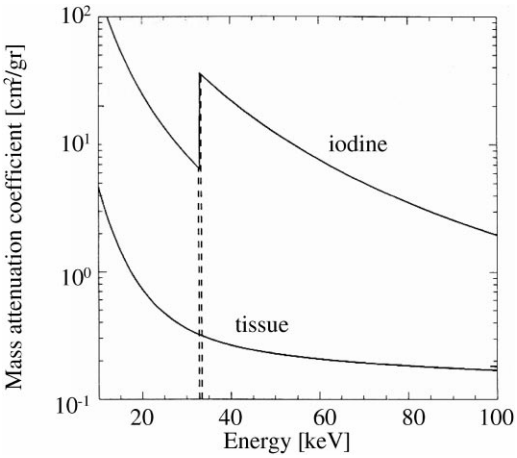

Fig. 2. Comparison between the mass attenuation coefficients of iodine and of water at the iodine K-edge.

obtains a system of two unknowns, namely the water image ($\rho_{\text{water}} x_{\text{water}}$) and the iodine image ($\rho_{\text{iodine}} x_{\text{iodine}}$) by the simple matrix inversion of

$$-\begin{pmatrix} S_1 \\ S_2 \end{pmatrix} = \begin{pmatrix} \dfrac{\mu^1_{\text{iodine}}}{\rho_{\text{iodine}}} & \dfrac{\mu^1_{\text{water}}}{\rho_{\text{water}}} \\ \dfrac{\mu^2_{\text{iodine}}}{\rho_{\text{iodine}}} & \dfrac{\mu^2_{\text{water}}}{\rho_{\text{water}}} \end{pmatrix} \begin{pmatrix} \rho_{\text{iodine}} & x_{\text{iodine}} \\ \rho_{\text{water}} & x_{\text{water}} \end{pmatrix} \quad (1)$$

where subscripts 1 and 2, respectively, refer to the energy below and above the iodine K-edge, S is the logarithmic and normalized images taken at the two energies, ρ, μ are the densities and absorption coefficients for water (tissue) and iodine and x describes the thickness of the specific material.

Several groups have taken various approaches to use synchrotron for intravenous coronary angiography with differences in X-ray optics and the types of digital detectors summarized in Table 1.

The concept of coronary angiography with synchrotron radiation was developed at Stanford University [5] and in 1979 the system was installed at the Stanford Synchrotron Radiation Laboratory (SSRL) where the first human studies were performed. In 1990 the equipment was moved to the Synchrotron Medical Research Facility (SMERF) at the National Synchrotron Light Source (NSLS) in Brookhaven where the experiments continued until 1996 [6]. The imaging system at NSLS was a 5 mm thick dual-linear lithium-drifted silicon detector with horizontal resolution of 250 μm while the vertical resolution was defined by the beam height [7].

Pioneering experiments at the Institute of Nuclear Physics in Novosibirsk (Russia) started in 1979 [8]. They used a double-line scintillation counter detector based on NaI scintillator crystals coupled with individual photo-multipliers working in single-photon counting mode with a counting rate of about 1 MHz per channel.

Different from other projects the programs at Photon Factory, Tsukuba (Japan), started in 1993, used a large beam obtained by an asymmetrically cut crystal and a two-dimensional detector. One example is the system working above the K-edge using an X-ray image intensifier and a CCD video camera [9].

The first experiments with the NIKOS system at HASYLAB at DESY (Germany) started in 1981 and between 1997 and 1999 the beamline was dedicated to extensive patient studies with some 400 patients [10] (Fig. 3). The focus here is to validate the diagnostic sensitivity and the medical impact with reasonable statistics. Until now this system is the most advanced. The detector consists of a two-line high-pressure $KrCO_2$ ionization chamber with a horizontal pixel size of 400 μm defined by the distance of the strips [11]. A comparison in terms of spatial frequency-depending DQE between the NIKOS and NSLS detectors has been performed [2].

At the medical imaging beamline at European Synchrotron Radiation Facility (ESRF), Grenoble (France) successful human studies started in the beginning of 2000 after preliminary results have been obtained on animals trials [12] (Fig. 4). A dual-line high-purity germanium detector (HPGe) with 350 μm pixel width made by Eurisys measures is used as an imaging device.

3. Bronchography

K-edge xenon dichromography for imaging the bronchial tree in humans is based on the same principle used for synchrotron radiation transvenous coronary angiography. Pilot studies [13] have been carried out on human volunteers at the SMERF facility at the NSLS using the same system

Table 1

Facility	Detector	Monochromator	Operation and status
SSRL Stanford (USA)	Dual line Si(Li) Integrating mode 5 mm thick, 500 μm pixel 4 ms integration time/line 14 bit dynamic	2 Si(1 1 1) Asymmetrical cut	Started in 1979 Animal and human studies In 1990 moved the equipment to NSLS
NSLS Brookhaven (USA)	Dual line Si(Li) Integrating mode 5 mm thick, 250 μm pixel 4 ms integration time/line 14 bit dynamic	1 bent LAVE Si(1 1 1)	Started in 1990 Human studies
VEPP-3 Novosibirsk (Russia)	Dual line scintillation counters Single photon counting mode Spatial resolution 0.1–2 mm 20 bits dynamic	2 LAVE Si(1 1 1)	Started in 1979 In vivo studies
Hasylab Hamburg (Germany)	Dual line ionization chamber Integrating mode 400 μm pixel Integration time 0.8 ms perline 19 bit dynamic	2 bent LAVE Si(1 1 1)	Started in 1981 Dedicated beamline for a large program on human studies since 1997
ESRF Grenoble (France)	Dual line HPGe Integrating mode 2 mm thick, 350 μm pixel integration time 0.8 ms per line 16 bit dynamic	1 bent LAVE Si(1 1 1)	Started in 1998 first animals. Human studies in the beginning of 2000
Photon Factory Tsukuba (Japan)	X-ray image Intensified + videocamera 2-dimension detector spatial resolution 250 μm Integration time 2 ms 9 bit dynamic	1 Si(3 1 1) Asymmetrical cut (large beam)	Started in 1983 In vivo studies Human studies in 1996

as that for angiography, which was reconfigured for the operation at the K-edge of xenon (34.56 keV). In this case a medical grade, non-radioactive xenon gas mixture (80% xenon, 20% oxygen) is used as a contrast agent. A time series of images above and below the xenon K-edge of xenon are taken simultaneously by the aforementioned Si(Li) dual line detector after the inhalation of the contrast agent. The bronchi down to the tertiary level were visible.

4. Computed tomography

A SR beam offers a suitable planar geometry for computer tomography (CT). In this case the sample is rotating while the laminar beam is crossing a slice of the object to be imaged. Due to the very small angular divergence the X-rays can be considered parallel and the detector has a simple linear geometry. Besides the ease of the geometry also the monochromaticity of the photon beam further simplifies the reconstruction [14] which is based on the assumption that the dependence from the energy of the attenuation coefficient does not change through the integration path. Thus artifacts due to beam hardening, which arise in normal tomography especially at the borders of high absorbing materials like bones and decrease the image quality, can be suppressed significantly. Another advantage is the possibility to choose the appropriate energy for a given size of the sample, resulting in larger signals for the same delivered dose.

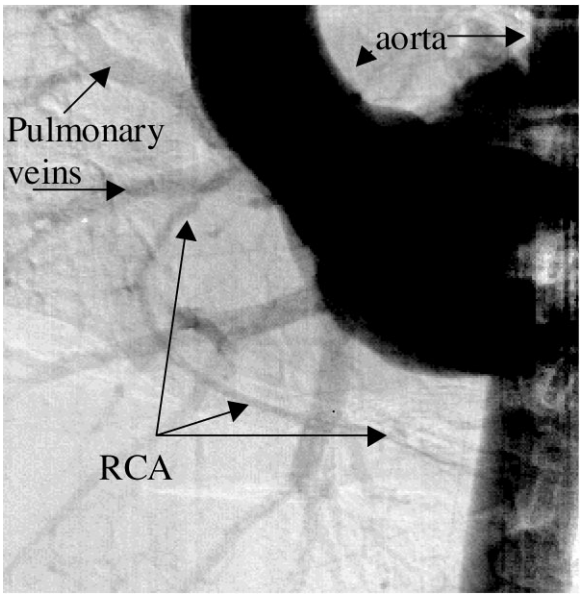

Fig. 3. A picture of a human heart obtained with subtraction coronary angiography at HASYLAB at DESY showing clearly the right coronary artery (RCA) after an intravenous injection of the contrast agent.

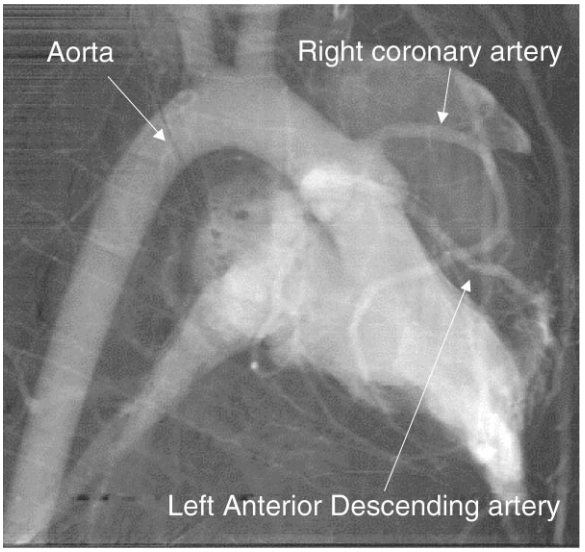

Fig. 4. First experiments for transvenous coronary angiography at the medical beamline at the ESRF: shown is the heart of a pig after an intravenous injection of the contrast agent.

Moreover multiple-energy imaging can be performed since the small-energy bandwidth allows energy-selective methods like K-edge subtraction (KES) imaging and dual-photon absorptiometry (DPA). The K-edge subtraction method (described in Section 3 for coronary angiography), can also be implemented for CT at the iodine K-edge for imaging the human neck, for example. However it is suboptimal for head imaging and impractical for chest or abdomen imaging because of the low transmission of the 33 keV X-rays. For whole-body CT the use of gadolinium as contrast agent (K-edge = 50.23 keV) is more suitable.

DPA is a subtraction method based on the different behavior of the photoelectric and Compton effects at two widely separated energies: two images have to be acquired, for instance at 40 and 100 keV. This method allows the differentiation of concentration of low- and intermediate-Z elements. DPA is also performed with X-ray tubes using filtered bremsstrahlung radiation for measuring bone mineral density, but the SR source can improve the image quality.

Multiple Energy Computer Tomography (MECT) was first developed at medical facility SMERF at NSLS with a program for imaging human neck and head with single- and dual-energy methods [15]. Experiments were carried out on phantoms and small mammals using a linear modular CdWO4-pin photodiode detector with a beam provided by two LAVE flat Si(1 1 1) crystals. DPA will be applied in the study of tissue characterization as carotid artery atherosclerotic plaque composition.

The CT program at ESRF [16] is focused on the evaluation of blood volume and tissuelar perfusion by concentration measurements of contrast agent in the brain in order to predict the outcome of cerebral ischemia and brain tumors. Here two bent LAVE Si(1 1 1) crystals are used as monochromator and the aforementioned high-purity germanium detector as imaging system.

In Tsukuba (Japan) a CT system has also been developed [17]. It was designed for performing KES with low-concentration contrast materials (iodine, barium, gadolinium) for research application like functional analysis imaging and bone mineral distribution imaging.

5. Mammography

Mammography is a screening technique with the highest sensitivity for detecting early breast cancer, which statistically leads to a significant improvement in breast cancer survival [18]. The demands on the image performance in mammography, in terms of contrast and resolution are beyond those of any other medical imaging modality. Subsequently the requirements on the X-ray source as well as on the detector are very high especially for the detection of low-contrast and small-size details such as clusters of micro-calcifications and low-contrast masses, possible indicators of early breast cancer. At the same time special care has to be taken for an efficient use of the radiation dose to the patient: since the breast is one of the most radiosensitive organs, the risk of cancer induced by X-ray exposure has to be minimized.

Since the first mammographic units became available in the 1970s several technology advancements have changed and have boosted both the equipment and the examination procedure with appropriate X-ray beam quality, adequate breast compression and automatic exposure control. Unfortunately, there are still several limitations and approximately 10% of the obvious clinical breast cancers are not visible with mammography [19].

The image quality is affected, besides the breast composition and thickness, by the radiation quality, the scattered radiation and the receptor performance.

The contrast of structures depends essentially on the difference of attenuation coefficient that, in case of normal and neoplastic breast tissue, can be in the order of few percent. In order to reveal these fine structures a dedicated X-ray source is required, since the optimization of the X-ray source can enhance the visibility of details. In conventional mammography a molybdenum target X-ray tube (Mo K-edge at 20 keV) in conjunction with a molybdenum filter is used. The energy spectrum consists of the typical continuous bremsstrahlung background with the 17.9 and 19.5 keV characteristic fluorescence line of the molybdenum target. The polychromatic spectrum can be modified changing the tube voltage. However, the best energy optimization can be achieved with a monoenergetic beam. This becomes obvious regarding the Figure of Merit (FOM), a parameter which describes the image quality versus the energy. According to Eq. (2) it is defined as the signal-to-noise ratio normalized to the mean glandular dose (MGD):

$$\mathrm{FOM} = \frac{\mathrm{SNR}}{\sqrt{\mathrm{MGD}}} \tag{2}$$

In an image where a detail is present in the background area the SNR measures the visibility of that detail and in the case of Poisson distribution it is defined as

$$\mathrm{SNR} = \frac{N_1 - N_2}{\sqrt{N_1}} \tag{3}$$

where N_1 is the average transmitted fluence of photons on the image in the background region and N_2 is the average transmitted fluence in the area of the detail. From Eq. (3) it turns out that the SNR is higher at lower energies because the difference of attenuation coefficients decreases with the energy. On the other hand lower energy means higher absorbed dose in the organ. Inserting Eq. (3) in Eq. (2) the FOM curve shows (Fig. 5) a maximum corresponding to a certain energy and consequently at that energy the image quality is maximized for the same radiation dose. Since the FOM

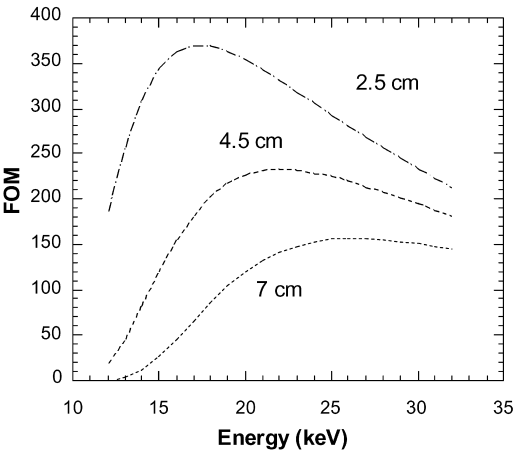

Fig. 5. The theoretical calculation of the Figure of Merit (FOM) for a detail of 5 mm diameter adipose tissue embedded in a breast with standard composition (50% adipose + 50% glandular) for different breast thicknesses.

depends on the tissue thickness and the tissue composition, a selectable monochromatic energy should be chosen according to the breast thickness and variation in the composition between more transparent adipose and denser glandular tissue. The example in Fig. 5 shows how the maximum moves to higher energies as the thickness of the sample increases.

Another important aspect is the beam geometry. In principle the spot size of the X-ray source should be pointlike to avoid penumbra effects increasing the image blurring. Moreover the wide-sized beam of an X-ray tube influences scattered radiation which decreases the contrast adding a uniform noisy background to the image. In order to reduce scattering anti-scatter grids are used. However, the insertion of the grid results in an increase of the radiation dose applied to the patient.

5.1. Synchrotron radiation mammography

In order to improve the source quality SR-based mammography experiments have been carried out. Comparing the energy spectrum of a SR source and of a mammographic X-ray tube it turns out that the SR intensity is orders of magnitude higher than that of a clinical unit. A monochromator can be utilized in order to obtain a beam with high flux and with a narrow energy bandwidth. The appropriate energy can be tuned according to the density and thickness of the breast. In addition the highly vertical collimated SR geometry reduce inherently the scattering in the image thus avoiding the use of anti-scatter grids. Approximately a decade ago a first pioneering work was done at ADONE (Frascati) using a channel-cut Si(1 1 1) crystal as monochromator and a conventional screen–film system [20]. The conclusion of these experiments was that the images of test objects as well as breast tissue specimens taken with the monochromatic SR have higher contrast resolution and similar or less radiation dose. Over the past years other preliminary investigations have been carried out by the medical research group at NSLS (Brookhaven) with screen–film and imaging plate detectors [21] and at SRS facility (Daresbury) with screen–film system [22] using in both cases flat Si(1 1 1) crystal monochromators.

Furthermore at NSLS additional studies for producing scatter-free images with the help of an analyzer crystal have been done. These studies opened the way to the DEI technique (see Section 7) based on the diffraction effects. Also at Daresbury diffraction imaging studies have shown the possibility of characterization of selected tissue types [23].

In order to fully validate and exploit the method a dedicated beamline for mammography called SYRMEP was designed and built at the SR facility ELETTRA, Trieste (Italy) and it is under operation since 1996 [24,25]. A Si(1 1 1) channel-cut crystal monochromator provides a 100 mm wide beam at the experimental hall in the energy range from 10 to 35 keV. The project studies the advantages of SR in mammography in conjunction with a novel digital detector based on a linear silicon array of pixels (see Section 6.2). Joining the SR features with the digital mammography approach promising experimental results have been obtained with both, phantoms and in-vitro full breast tissue samples (Fig. 6). For comparison images were taken with the digital detector as well as a classical clinical screen–film cassette [26]. For the images taken with the digital detector the applied dose to the sample was smaller or comparable to that of the clinical unit, however in terms of contrast resolution the digital ones are superior.

According to the specific experimental requirements the fan-like beam is first monochromized and then is shaped by a micro-metric tungsten slit system in the experimental hall. When using the linear digital detector the beam height has to match the vertical pixel size to avoid undesirable dose delivered to the sample. In all the SR based mammography experiments the image acquisition is obtained scanning the sample through the beam due to the laminar shape of the beam.

6. Screen–film system limitations and digital mammography

Screen–film systems are currently dominating the market and offer excellent detection capabilities. However several limitations still affect these detection systems [27].

Fig. 6. An in-vitro full breast tissue sample image acquired at 20 keV with the digital detector at the SYRMEP beamline at ELETTRA.

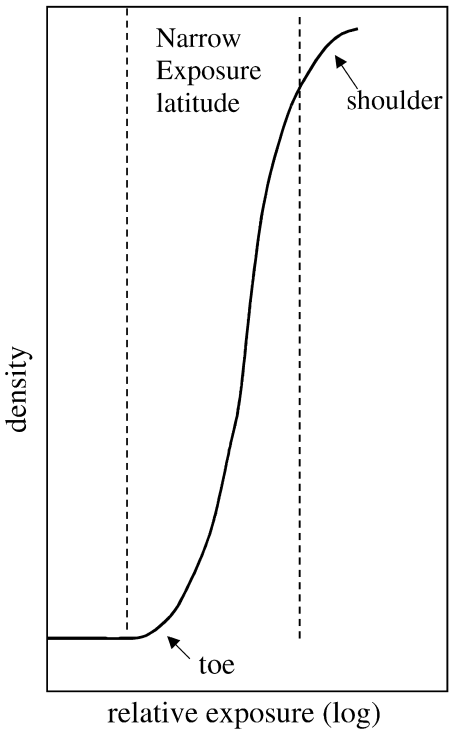

Fig. 7. A characteristic curve of a screen–film system with the typical sigmoidal shape.

One of the main drawbacks of film is its non-linear response. The contrast properties of a radiographic film are described by its characteristic curve (Fig. 7) which has typically a sigmoidal shape. This means that the range of the X-ray exposure with linear correspondence with the optical density is limited to a factor of about 25.

The noise in this system is due to the structure of the fluorescent screen and, mainly, to the granularity of the film emulsion that prevents the system to be 'quantum limited' decreasing the contrast resolution.

An important challenge in screen-film mammography is the capability to diagnose early stages of breast cancer in radiologically dense breast (or breast types that contain a large amount of fibroglandular tissue). Subtle attenuation variation in breast tissue requires a high contrast sensitivity that means a steep slope in the characteristic curve of the film. On the other hand a trade-off between the contrast sensitivity and the film dynamic range (latitude) has to be considered. High contrast sensitivity is not suitable for a large range of transmitted exposure due to the presence of dense (radiographically opaque) and adipose (transparent) part in breast composition. As a consequence dense parts can be underexposed or transparent parts can be overexposed corresponding to the toe and to the shoulder of the characteristic curve.

Another limitation of screen-film mammography is the compromise between spatial resolution and X-ray interaction efficiency. To perform a radiograph at a reasonable dose the film is used in contact with a fluorescent screen that converts the X-rays in the visible light. The absorption efficiency depends on the phosphor thickness, but as the thickness increases also the screen blur increases reducing the spatial resolution. This is due to the

diffusion of light from the point of absorption of the X-ray to the film. In mammography high spatial resolution (18–20 lp/mm) is essential thus the screen must be relatively thin with a consequent reduction of the detection efficiency.

The contrast resolution is also affected by the intrinsic noise of this system which is due to the structure of the fluorescent screen and, mainly, to the granularity of the film emulsion that prevents the system to be 'quantum limited'. The DQE of screen–film system reaches a maximum of 0.25–0.50 at low spatial frequencies and drops to less than 1% at higher frequencies [28]. The loss of DQE is attributable primarily to film granularity noise.

In the digital approaches several limitations can be overcome [27–29]. It should be pointed out that in digital mammography the image acquisition, display and storage are performed independently allowing optimization of each procedure. The response of detector is linear over a much wider dynamic range (12 bits or more), therefore more ideal for radiologically dense breast types with improved lesion detectability.

To fulfil the severe requirements of mammography the digital detectors must feature low intrinsic noise and a very high detection efficiency in order to keep the dose to minimum necessary, hence, a high DQE system is necessary.

Furthermore, in a digital system the exposure is terminated when a sufficient signal-to-noise ratio is obtained and it is not defined by the optical density of the film. The spatial resolution should be also very high and reasonable pixel size is supposed to be about 100–50 μm^2. Moreover, a digital image presents all the advantages of the computer manipulations to improve the detectability of subtle and small suspicious lesions with off-line contrast enhancement procedures.

6.1. Full-field detectors

The main challenge in digital detector development is the implementation of a large area (to be comparable to the $18 \times 24\,cm^2$ field size of the mammographic film cassette) together with a high spatial resolution. Different solid-state detectors could be available for this purpose, but it is not a trivial problem to design one that could produce a full breast image with resolution matching that of the screen–film system (18–20 lp/mm). All the detectors under development have a spatial resolution lower than that of the film. However the better contrast resolution achieved in all cases is expected to compensate for the reduced spatial resolution. Different approaches are pursued in detector design employing either area or linear solid-state devices [27–30].

Small charge-coupled devices (CCDs) for stereotactic breast biopsy with a limited field of view have been available for several years and recently a development of these systems has lead to new designs for full field of view mammography. They all work in indirect-conversion mode that means they utilize a scintillator, which is coupled with the CCD by means of a fiber-optic taper to convert the X-rays into visible light. If an unstructured phosphor scintillator is used the trade-off between spatial resolution and absorption efficiency, correlated with its thickness, must be kept in mind. Several systems have employed columnar-structured cesium iodide scintillators with a reduced lateral spread of the light.

One approach is to use a mosaic of 12 (3×4) charge-coupled devices (CCDs) bonded together and coupled to an $18 \times 24\,cm^2$ cesium-iodide scintillator to create a large imaging area [31]. Another method is a slot–beam system, a good compromise between an area and a linear detector, developed by the University of Toronto [32–34]. In the prototype unit a gadolinium phosphor screen and a 2:1 demagnifying fiber-optic taper and a pixel of $50\,\mu m^2$ was used. The scanned-slot mechanism consists of a fan-shaped beam of mammographic X-ray tube scanned in continuous mode over the breast simultaneously with a slot-shaped CCD detector. This system can reduce the amount of scattered radiation in the image without the use of grids. Of course, in order to complete the scan without a longer exposure time, the X-ray flux must be increased compared to that used with an area detector. For this systems a time-delay integration (TDI) technique is applied in order to allow a smooth mechanical movement and an averaging of pixel response (defects and dishomogeneities) in the row along the scan direction [29,34,35]. As the detector and the fan-shaped beam are scanned across the

breast the charges collected in each pixel are shifted in the opposite direction and synchronized at the same speed as that of the scan.

In a more recent development cesium-iodide is coupled to a slot-scan CCD detector in TDI mode with $1.0 \times 24\,cm^2$ sensitive area [36]. The DQE exceeds 50% and the pixel size is $50 \times 50\,\mu m^2$.

Another method for full-field mammography is based on the use of large-area, flat-panel amorphous-silicon image sensors that have recently been developed for X-ray imaging applications (radiography and fluoroscopy) [37,38]. The development in the technology of amorphous silicon is primarily due to the commercial interest in flat-panel displays. They offer the advantage (with respect to crystalline silicon) to be fabricated at reasonable low cost in large sheet ($20 \times 25\,cm^2$), recently covering an area up to $30 \times 40\,cm^2$ [39]. They can achieve a high DQE (around 65–75%) and a wide dynamic range. Recently high spatial resolution with a pixel size of about $(100\,\mu m)^2$ has been achieved [40].

These active-matrix, flat-panel imagers consist of an array of pixels, each one formed by a single-amorphous-silicon (a-Si:H) thin-film transistor (TFT) which is coupled with a discrete a-Si:H n–i–p photodiode working in indirect-conversion mode. As in the case of the previously discussed CCD detectors a scintillator such as a phosphor or cesium-iodide is coupled to the flat panel (Fig. 8).

The electronic signal accumulated in each pixel capacitance is read-out by the TFT switches connected to the gate lines and the source lines [29] (Fig. 9). When one gate line is activated all the TFTs in that row are switched on and the signals from all the pixels in the row can be read-out by the source lines. Because of its architecture the active fraction (fill factor) of the pixel is less then 100% and decreases with the pixel size resulting in a limit for the spatial resolution (35% for $(127\,\mu m)^2$ pixel [28]). However very recent studies [41] describe a new design for an amorphous silicon sensor array with a pixel size of about $(70\,\mu m)^2$ with a high fill factor.

In the last few years growing interest and progress have been reported on the development of direct-detection selenium flat-panel digital radiographic imaging devices [42,43]. An amorphous selenium photo-conductor layer is coated over a TFT readout active matrix.

The charges, generated by means of photoelectric interaction of the X-rays with the selenium layer, are integrated on storage capacitors that are located at each pixel. A high electric field (typically $10\,V/\mu m$) must be applied across selenium to collect charges and to avoid their recombination. In this way the lateral spreading of the signal is minimized resulting in a high spatial resolution.

A $500\,\mu m$ thick selenium device has been developed [44]. It has large active imaging area ($35 \times 43\,cm^2$) with a pixel size of $(139\,\mu m)^2$ and a high fill factor of 86%.

Selenium detector prototypes with a design suitable for digital mammography performing high DQE and high special resolution (optimized

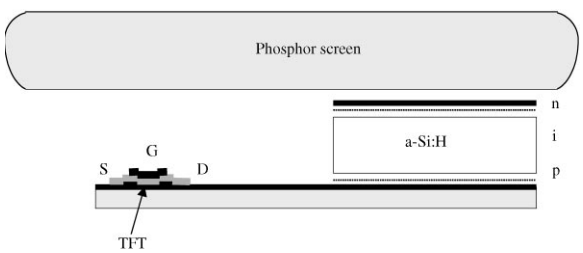

Fig. 8. A schematic layout of a pixel in an amorphous silicon flat panel detector.

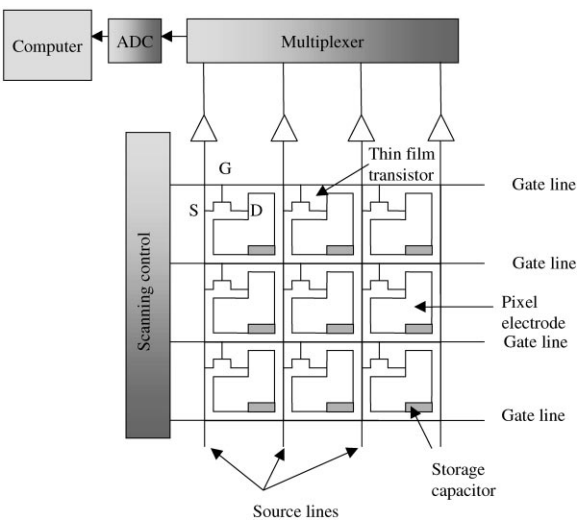

Fig. 9. The scheme of an active matrix of Thin Film Transistor (TFT). For description see text.

conversion layer thickness and pixel size smaller than $(100\,\mu m)^2$) are currently under study [45–48].

6.2. The digital detector at the SYRMEP beamline

The digital detector utilized at the SYRMEP beamline at ELETTRA for mammography consists of a micro-strip silicon detector made by Canberra which is irradiated from the side in an 'edge on' geometry [49]. In this configuration it acts as a linear pixel detector with a horizontal pixel size of 200 μm defined by the strip pitch and a vertical pixel size of 300 μm due to the wafer thickness. This configuration allows an absorption efficiency of about 100% in the energy range of interest since the beam impinges parallel to the longitudinal dimension (10 mm) of the strips which becomes the effective detector thickness. This pixel depth ensures a high detection efficiency (about 80% for X-rays at 20 keV) which is anyway lower than the absorption efficiency because of the presence of an insensitive volume. This is due to the fact that the strips are implanted 250 μm from the edge [50]. A single-layer detector consists of an array of 256 strips covering an area of $51.2 \times 0.3\,mm^2$.

The electronics works in single-photon counting mode; hence the detector is 'quantum limited' because the image noise is only due to the photon Poisson statistics resulting in a high dynamic range and in a better contrast resolution. The readout electronics is realized in the form of a low noise VLSI chip [51], which is made by LEPSI (Strasbourg). It is a 32-channel mixed analogue-digital cell custom designed for applications requiring low-noise amplification and counting of single pulses. Each channel features an analogue part, which consists of a charge-sensitive preamplifier, a CR-RC shaping amplifier, an analogue buffer, a threshold discriminator, and a 16 bit pulse counter. The read-out of all counters in the circuit is done in serial up to a rate of 20 MHz. The counting rate using periodic signals is close to 100 kHz. During the data acquisition, however, it is kept lower (about 10 kHz) to avoid partial saturation of the read-out chain due to the statistical time distribution of the photons.

In order to achieve a shorter acquisition time a multilayer detector with a larger sensitive area has been implemented [52]. To allow the stacking of devices one on the top of each other the SYRMEP detector was produced in a special design. The first 'stacked' assembly prototype consists of three layers covering a cross section of about $50 \times 1\,mm^2$ (Fig. 10).

7. New imaging techniques

In the recent years with the increasing use of synchrotron sources several researchers have investigated the potential of different imaging techniques based on phase effects. The contrast enhancement in comparison with the normal absorption techniques can be achieved by exploiting refraction differences in those heterogeneous samples, which normally show only little absorption contrast. These differences can be related to a phase shift of the incident wave field propagating inside the sample and can be described with corresponding variations in the real part of the complex refractive index $n = 1 - \delta + i\beta$. In the energy range suitable for the X-ray imaging of biological samples they can be considerably larger ($\sim 10^3$) than the imaginary ones, which are related to the absorption.

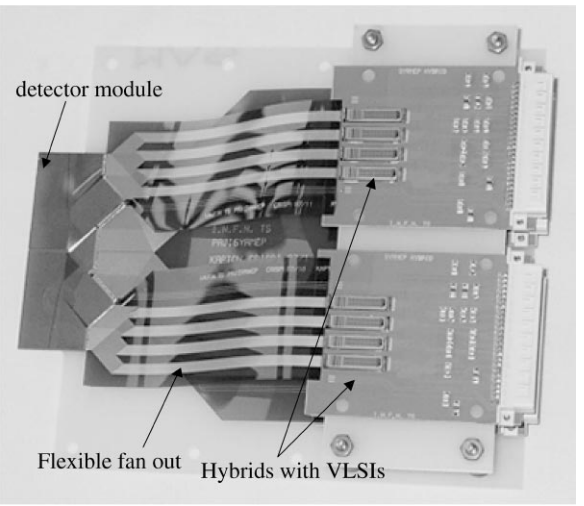

Fig. 10. A picture of the three-layer SYRMEP detector during the assembly of the first two layers: visible are the silicon strip detector, the fan-out and the electronics.

One modality that exploits these phase effects is the Phase Contrast "in line" imaging method that requires high spatial coherence of the X-ray source like micro-focus X-ray tubes or SR sources [53–55].

Unlike in optical in-line holography the phase information is converted here into an intensity information generated by the interference between an unperturbated reference wave field and a wave field diffracted by small objects inside the sample. Since a larger gradient of the refractive index is present at the borders of those details this technique produces a tremendous edge enhancement effect in the images. The intensity information that can be resolved is just a question of the right distance between the sample and the detector and eventually of the spatial resolution.

Usually the detectors utilized for this technique have a very high resolution; hence a high radiation dose is delivered to the sample. However, studies on mammographic phantoms and breast tissue samples at the SYRMEP beamline at ELETTRA have demonstrated the possibility of performing phase contrast imaging using clinical mammographic screen–film system. That means an improved detail visibility with a dose fully comparable to the clinical one [56] (Fig. 11).

A phase contrast X-ray-computed tomography method for observing biological soft tissue has been recently developed and demonstrated by Momose following an idea of using an X-ray Bonse–Hart-type interferometer [57,58].

Another technique considers that a phase gradient across a wavefront is equivalent to a variation in the direction of propagation of the wave. These variations can be resolved with an analyzer crystal of high angular sensitivity due to its narrow reflectivity curve [59,60]. One of those methods is called Diffraction Enhanced Imaging (DEI) and was developed at NSLS for mammography with improved image contrast [61]. DEI is based on the use of an analyzer crystal and a post-processing elaboration. It is capable of producing images of the refraction and absorption independently in a sample acquiring two images, one on the left and one on the right hand side of the crystal reflectivity curve. Images of a standard mammographic phantom and breast tissue sample have been obtained using a Si(3 3 3) crystal.

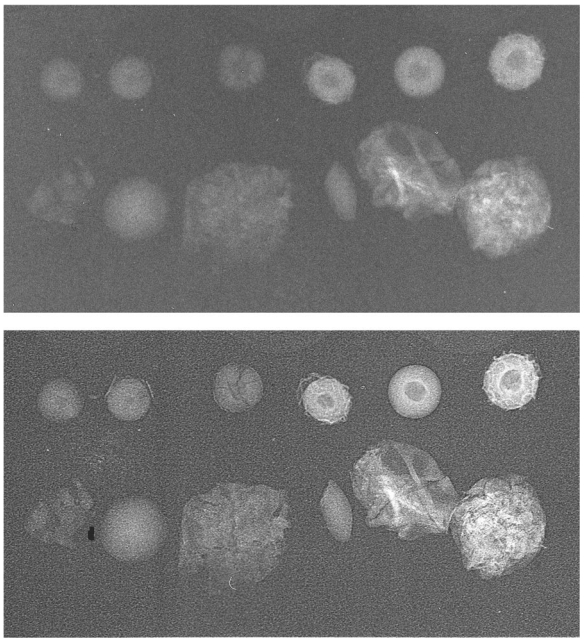

Fig. 11. Simulated tissue in a mammographic phantom obtained with a clinical mammographic unit (upper image) and at the SYRMEP beamline (ELETTRA) with the phase contrast technique at 20 keV (lower image). In both cases the same clinical screen–film system was used with a comparable dose.

Studies of diffraction imaging with phantoms and breast tissues using a Si(1 1 1) analyzer imaging crystal have been carried out at the SYRMEP beamline at ELETTRA [62]. A clinical screen–film cassette and a Fuji BAS 1800 imaging plate system featuring a pixel size of 50 μm have been used as detectors. Images obtained with the analyzer perfectly aligned with the primary monochromator are in principle scatter-free while the images obtained with different degrees of misalignment show a weighted contribution of the transmitted beam and of the beam refracted at a certain angle. As an example the radiographs of nylon strings of 100 μm diameter and quartz spheres of 150 μm diameter are depicted in Fig. 12. The X-ray energy was set to 17 keV and in all three cases the applied dose was almost the same. Note that in the transmission image the strings are not visible while the images taken with the analyzer show all the details including the strings with a high SNR.

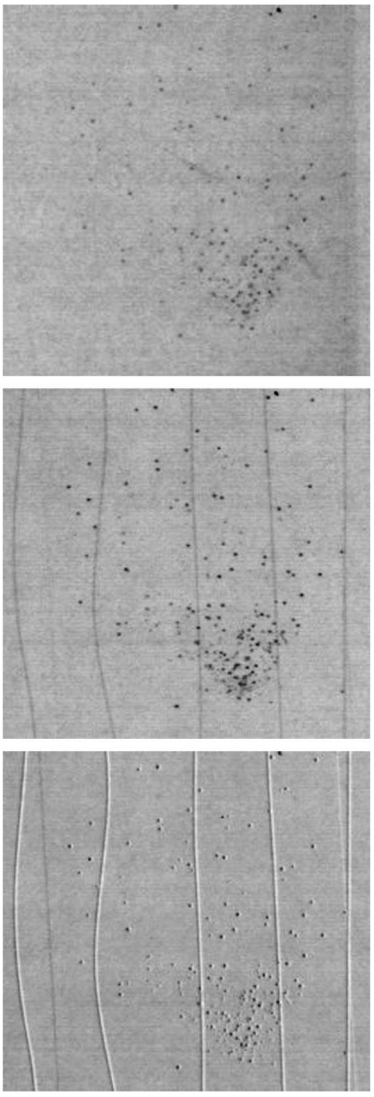

Fig. 12. Images of 100 μm nylon wires and 150 μm quartz spheres obtained at the SYRMEP beamline (ELETTRA) in transmission geometry (upper image), with the analyzer aligned with the primary monochromator (middle) and with a misaligned analyzer (lower).

8. Summary

X-ray synchrotron radiation sources have a widespread field of interest and in the past years it was demonstrated that synchrotron radiation is a powerful tool in medical/radiological applications. Coronary angiography is the most advanced medical application and recently the validity of the method has been tested on human patients in a large program at HASYLAB at DESY. Clearly mammography can take advantage of the peculiar characteristic of the synchrotron radiation sources. In order to fulfil the demanding requirements of these experimental researches a big effort in a parallel development of imaging system technology with digital detector and electronics has to be launched. In particular, crucial will be the full-field digital mammography and different solutions have been investigated. Some systems produced for standard medical X-ray equipment are already commercially available. For SR-based full-field mammography a novel 'edge on' Si-strip detector has been developed.

Recently new promising phase imaging modalities have been developed which can highly enhance the image contrast hence opening interesting perspective also in medical diagnostic imaging. Here synchrotron light offers a suitable X-ray source to advance these techniques.

Acknowledgements

I would like to thank the members of the organizing committee of the SAMBA Conference for their kind invitation and their warm hospitality. It is a pleasure for me to thank Dr. H.J. Besch for many enlightening discussions and for the good times during the common experiments.

All my gratefulness are due to Dr. R.H. Menk for all the interesting discussions and all his teaching and advises from his experience in SR applications and detectors. A special thanks for his careful revision of my paper.

I am indebted to Dr. W. Thomlinson and the other researchers of the medical facility at NSLS from whom I gained a fundamental experience in SR medical applications and my knowledge of the DEI technique.

I would like to thank Prof. E. Castelli and all my colleagues and friends for all the important work we have done together at the SYRMEP beamline.

References

[1] R. Lewis, Phys. Med. Biol. 42 (1997) 1213.

[2] R.H. Menk, W. Thomlinson, N. Gmür, Z. Zhong, D. Chapman, F. Arfelli, W.R. Dix, W. Graeff, M. Lohmann, G. Illing, L. Schildwaechter, B. Reime, W. Kupper, C. Hamm, J.C. Giacomini, H.J. Gordon, E. Rubenstein, J. Dervan, H.J. Besch, A.H. Walenta, Nucl. Instr. and Meth. A 398 (1997) 351.

[3] W. Kupper, Internist. 31 (1990) 341.

[4] D. Chapman, C. Schulze, IEEE Conference Report, Nuclear Science Symposium & Medical Imaging Conference, Vol. III, 1993, p. 1528.

[5] E. Rubenstein, R. Hofstadter, H.D. Zeman, A.C. Thompson, J.N. Otis, G.S. Brown, J.C. Giacomini, H.J. Gordon, R.S. Kernoff, D.C. Harrison, W. Thomlinson, Proc. Natl. Acad. Sci. USA 83 (1986) 9724.

[6] W. Thomlinson, N. Gmür, D. Chapman, R. Garrett, N. Lazarz, H. Moulin, A.C. Thompson, H.D. Zeman, G.S. Brown, J. Morrison, P. Reiser, V. Padmanabahn, L. Ong, S. Green, J. Giacomini, H. Gordon, E. Rubenstein, Rev. Sci. Instr. 63 (1992) 625.

[7] A.C. Thompson, W.M. Lavender, D. Chapman, N. Gmür, W. Thomlinson, V. Rosso, C. Schulze, E. Rubenstein, J.C. Giacomini, H.J. Gordon, Nucl. Instr. and Meth. A 347 (1994) 545.

[8] E.N. Dementyev, E.Ya. Dovga, G.N. Kulipanov, A.S. Medvedko, N.A. Mezentsev, V.F. Pindyurin, M.A. Sheromov, A.N. Skrinsky, A.S. Sokolov, V.A. Ushakov, E.I. Zagorodnikov, Nucl. Instr. and Meth. A 246 (1986) 726.

[9] T. Takeda, Y. Itai, J. Wu, S. Ohtsuka, K. Hyodo, M. Ando, K. Nishimura, S. Hasegawa, T. Akatsuka, M. Akisada, Acad. Radiol. 2 (1995) 602.

[10] C.W. Hamm, T. Meinertz, W.R. Dix, C. Rust, W. Graeff, G. Illing, M. Lohmann, R. Menk, B. Reime, L. Schildwachter, H.J. Besch, W. Kupper, Hertz 21 (1996) 127.

[11] R.H. Menk, W.R. Dix, W. Graeff, G. Illing, B. Reime, L. Schildwaechter, U. Tafelmeier, H.J. Besch, U. Grossmann, R. Langer, M. Lohmann, H.W. Schenk, M. Wagner, A.H. Walenta, W. Kupper, C. Hamm, C. Rust, Rev. Sci. Instr. (1994) 2235.

[12] H. Elleaume, A.M. Charvet, P. Berkvens, G. Berruyer, T. Brochard, T. Dabin, M.C. Dominguez, A. Draperi, S. Fiedler, G. Goujon, G. Le Duc, M. Mattenet, C. Nemoz, M. Perez, M. Renier, C. Schulze, P. Spanne, P. Suortti, W. Thomlinson, F. Esteve, B. Bertrand, J.F. Bas, Nucl. Instr. and Meth. A 428 (1999) 513.

[13] J.C. Giacomini, H. Gordon, R. ONeil, A. Van Kessel, B. Carson, D. Chapman, W. Lavendar, N. Gmür, R. Menk, W. Thomlinson, Z. Zhong, E. Rubenstein, Nucl. Instr. and Meth. A 406 (1998) 473.

[14] F.A. Dilmanian, Am J Physiol imaging 3/4 (1992) 175.

[15] F.A. Dilmanian, X.Y. Wu, E.C. Parsons, B. Ren, J. Kress, T.M. Button, L.D. Chapman, J.A. Coderre, F. Giron, D. Greenberg, D.J. Krus, Z. Liang, S. Marcovici, M.J. Petersen, C.T. Roque, M. Shleifer, D.N. Slatkin, W.C. Thomlinson, K. Yamamoto, Z. Zhong, Phys. Med. Biol. 42 (1997) 371.

[16] A.M. Charvet, C. Lartizien, F. Esteve, G. Le Duc, A. Collomb, H. Elleaume, S. Fiedler, A. Thompson, T. Brochard, U. Kleuker, H. Steltner, P. Spanne, P. Suortti, J.F. Le Bas, in: M. Ando, C. Uyama (Eds.), Medical Applications of Synchrotron Radiation, Springer, Berlin, 1998, p. 95.

[17] Y. Itai, T. Takeda, T. Akatsuka, T. Maeda, K. Hodo, A. Uchida, T. Yuasa, M. Kazama, J. Wu, M. Ando, Rev. Sci. Instr. 66 (2) (1995) 1385.

[18] M.J. Yaffe, Syllabus: a categorical course in physics, technical aspects of breast imaging, in: A.G. Haus, M.J. Yaffe (Eds.), Oak Brook, Vol. III, Radiological Society of North America, 1994, p. 275.

[19] NCRP Report no. 85, National Council on Radiation protection and Measurements, Washington DC, 1986.

[20] E. Burattini, E. Cossu, C. Di Maggio, M. Gambaccini, P. Indovina, M. Marziani, M. Porek, S. Simeoni, G. Simonetti, Radiology 125 (1994) 239.

[21] R.E. Johnston, D. Washburn, E. Pisano, C. Burns, W.C. Thomlinson, L.D. Chapman, F. Arfelli, N. Gmür, Z. Zhong, D. Sayer, Radiology 200 (1996) 659.

[22] R.A. Lewis, A.P. Hufton, C.J. Hall, W.I. Helsby, E. Towns-Andrews, S. Slawson, C.R.M. Boggis, Synch. Rad. News 12 (1999) 7.

[23] R.A. Lewis, K.D. Rogers, C.J. Hall, E. Towns-Andrews, S. Slawson, A. Evans, S.E. Pinder, I.O. Ellis, C.R.M. Boggis, A. Hufton, D.R. Dance, Proc. SPIE 3770 (1999) 32.

[24] F. Arfelli, G. Barbiellini, V. Bonvicini, A. Bravin, G. Cantatore, E. Castelli, L. Dalla Palma, M. Di Michiel, R. Longo, A. Olivo, S. Pani, D. Pontoni, P. Poropat, M. Prest, G. Richter, R. Rosei, M. Sessa, G. Tromba, R. Turchetta, A. Vacchi, Physica Medica XIII (Suppl 1) (1997) 7.

[25] F. Arfelli, A. Bravin, G. Barbiellini, G. Cantatore, E. Castelli, M. Di Michiel, P. Poropat, R. Rosei, M. Sessa, A. Vacchi, L. Dalla Palma, R. Longo, S. Bernstorff, A. Savoia, G. Tromba, Rev. Sci. Instr. 66 (1995) 1325.

[26] F. Arfelli, V. Bonvicini, A. Bravin, G. Cantatore, E. Castelli, L. Dalla Palma, M. Di Michiel, R. Longo, A. Olivo, S. Pani, D. Pontoni, P. Poropat, M. Prest, A. Rashevsky, G. Tromba, A. Vacchi, Radiology 208 (1998) 709.

[27] S.A. Feig, M.J. Yaffe, Digital Mammograph. Radiogr. 18 (1998) 893.

[28] M.B. Williams, L.L. Fajardo, Acad. Radiol. 3 (1996) 429.

[29] M.J. Yaffe, J.A. Rowlands, Phys. Med. Biol. 42 (1997) 1.

[30] H.G. Chotas, J.T. Dobbins, C.E. Ravin, Radiology 210 (1999) 595.

[31] L. Cheung, R.A. Coe, Med. Electron. 50 (1995).

[32] R.M. Nishikawa, G.E. Mawdsley, A. Fenster, M.J. Yaffe, Med. Phys. 14 (1987) 717.

[33] A.D. Maidment, M.J. Yaffe, Proc. SPIE 1231 (1990) 316.

[34] A.D. Maidment, J.M. Yaffe, D.B. Plewes, G.E. Mawdsley, I.C. Soutar, B.G. Starkoski, Proc. SPIE 1896 (1993) 93.

[35] E. Toker, M.F. Piccaro, Proc. SPIE 2009 (1993) 246.

[36] B. Munier, G. Roziere, J. Chabbal, Proc. SPIE 2432 (1995) 386.
[37] L.E. Antonuk, J. Boudry, Y. El-Mohri, W. Huang, J.H. Siewerdsen, J. Yorkston, R.A. Street, Proc. SPIE 2163 (1994) 118.
[38] L.E. Antonuk, J. Yorkston, H. Weidong, J.H. Siewerdsen, J.M. Boudry, Y. El-Mohri, M.V. Marx, Radiographics 15 (1995) 993.
[39] R.L. Weisfield, M.A. Hartney, R.A. Street, R.B. Apte, Proc. SPIE 3336 (1998) 444.
[40] L.E. Antonuk, Y. El-Mohri, A. Hall, K.W. Jee, M. Maolinbay, S.C. Nassif, X. Rong, J.H. Siewerdsen, Q. Zhao, R.L. Weisfield, Proc. SPIE 3336 (1998) 2.
[41] J.T. Rahn, F. Lemmi, R.L. Weisfield, R. Lujan, P. Mei, J.P. Lu, J. Ho, S.E. Ready, R.B. Apte, P. Nylen, J.B. Boyce, R.A. Street, Proc. SPIE 3659 (1999) 510.
[42] W. Zhao, J.A. Rowlands, Med. Phys. 22 (1995) 1595.
[43] D.L. Lee, L.K. Cheung, L.S. Jeromin, Proc. SPIE 2432 (1995) 237.
[44] D.L. Lee, L.K. Cheung, Rodricks, G. Brian, G.F. Powell, Proc. SPIE 3336 (1998) 14.
[45] R. Fahrig, J.A. Rowlands, M.J. Yaffe, Med. Phys. 22 (1995) 153.
[46] W. Zhao, J.A. Rowlands, S. Germann, D. Waechter, Z.Z. Huang, Proc. SPIE 2432 (1995) 250.
[47] M.P. Andre, B.A. Spivey, P.J. Martin, A.L. Morsell, E. Atlas, T. Pellegrino, Proc. SPIE 3336 (1998) 204.
[48] B. Polischuk, H. Rougeot, K. Wong, A. Debrie, E. Poliquin, M. Hansroul, J. Martin, T. Truong, M. Choquette, L. Laperriere, Z. Shukri, Proc. SPIE 3659 (1999) 417.
[49] F. Arfelli, V. Bonvicini, A. Bravin, P. Burger, G. Cantatore, E. Castelli, M. Di Michiel, R. Longo, A. Olivo, S. Pani, D. Pontoni, P. Poropat, M. Prest, A. Rashevsky, G. Tromba, A. Vacchi, N. Zampa, Nucl. Instr. and Meth. A 385 (1997) 311.
[50] F. Arfelli, G. Barbiellini, V. Bonvicini, A. Bravin, G. Cantatore, E. Castelli, M. Di Michiel, R. Longo, A. Olivo, S. Pani, D. Pontoni, P. Poropat, M. Prest, A. Rashevsky, G. Tromba, A. Vacchi, N. Zampa, IEEE Trans. Nucl. Sci. NS- 44 (1997) 874.
[51] G. Comes, F. Loddo, Y. Hu, J. Kaplon, F. Ly, R. Tuchetta, V. Bonvicini, A. Vacchi, Nucl. Instr. and Meth. A 377 (1996) 440.
[52] F. Arfelli, V. Bonvicini, A. Bravin, G. Cantatore, E. Castelli, L. Dalla Palma, R. Longo, A. Olivo, S. Pani, P. Poropat, M. Prest, A. Rashevsky, L. Rigon, G. Tromba, A. Vacchi, E. Vallazza, Proc. SPIE 3659 (1999) 817.
[53] S.W. Wilkins, T.E. Gureyev, D. Gao, A. Pogany, A.W. Stevenson, Nature 384 (1996) 335.
[54] A. Snigirev, I. Snigireva, V. Kohn, S. Kuznetsov, I. Schelokov, Rev. Sci. Instr. 66 (1995) 5486.
[55] P. Cloetens, R. Barrett, J. Baruchel, J. Guigay, M. Schlenker, J. Phys. D: Appl. Phys. 29 (1996) 133.
[56] F. Arfelli, M. Assante, V. Bonvicini, A. Bravin, G. Cantatore, E. Castelli, L. Dalla Palma, M. Di Michiel, R. Longo, A. Olivo, S. Pani, D. Pontoni, P. Poropat, M. Prest, A. Rashevsky, G. Tromba, A. Vacchi, E. Vallazza, F. Zanconati, Phys. Med. Biol. 43 (1998) 2845.
[57] A. Momose, Nucl. Instr. and Meth. A 352 (1995) 622.
[58] A. Momose, T. Takeda, Y. Itai, Rev. Sci. Instr. 66 (1995) 1434.
[59] T.J. Davis, D. Gao, T.E. Gureyev, A.W. Stevenson, W. Wilkins, Nature 373 (1995) 595.
[60] V.N. Ingal, E.A. Beliaevskaya, J. Phys. D 28 (1995) 2314.
[61] D. Chapman, W. Thomlinson, R.E. Johnson, D. Washburn, E. Pisano, N. Gmür, Z. Zhong, R. Menk, F. Arfelli, D. Sayers, Phys. Med. Biol. 42 (1997) 2015.
[62] F. Arfelli, V. Bonvicini, A. Bravin, G. Cantatore, E. Castelli, L. Dalla Palma, R. Longo, R. Menk, A. Olivo, S. Pani, P. Poropat, M. Prest, A. Rashevsky, L. Rigon, G. Tromba, A. Vacchi, E. Vallazza, Proc. SPIE 3770 (1999) 2.